Stable maintenance of the rudivirus SIRV3 in a carrier state in *Sulfolobus islandicus* despite activation of the CRISPR-Cas immune response by a second virus SMV1

Pavlos Papathanasiou[1]*, Susanne Erdmann[1,3]*, Carlos Leon-Sobrino[1,4]*, Kundan Sharma[2,5], Henning Urlaub[2], Roger A. Garrett[1] and Xu Peng[1,#]

[1] Danish Archaea Centre, Department of Biology, University of Copenhagen, DK2200 Copenhagen N, Denmark

[2] Max Planck Institute of Biophysical Chemistry, Am Faßberg 11, D37077 Göttingen, Germany Bioanalytics Research Group, Institute of Clinical Chemistry, University Medical Center Göttingen, Göttingen, Germany.

Present addresses:

[3] ithree Institute, University of Technology Sydney, Sydney, New South Wales, Australia

[4] Centre for Microbial Ecology and Genomics, Department of Genetics, University of Pretoria, 0028 Hatfield, Pretoria, South Africa

[5] Ludwig Institute for Cancer Research, University of Oxford, Old Road Campus Research Building, Roosevelt Drive, Oxford, OX37DQ, UK

* The authors contributed equally

Corresponding author - Xu Peng at peng@bio.ku.dk

Disclosure of potential conflicts of interest

There were no conflicts of interest and no financial benefits from the work

ABSTRACT

Carrier state viral infection constitutes an equilibrium state in which a limited fraction of a cellular population is infected while the remaining cells are transiently resistant to infection. This type of infection has been characterized for several bacteriophages but not, to date, for archaeal viruses. Here we demonstrate that the rudivirus SIRV3 can produce a host-dependent carrier state infection in the model crenarchaeon *Sulfolobus*. SIRV3 only infected a fraction of a *Sulfolobus islandicus* REY15A culture over several days during which host growth was unimpaired and no chromosomal DNA degradation was observed. CRISPR-Cas spacer acquisition from SIRV3 DNA was induced by coinfecting with the bicaudavirus SMV1 and it was coincident with increased transcript levels from subtype I-A adaptation and interference *cas* genes. However, this response did not significantly affect the carrier state infection of SIRV3 and both viruses were maintained in the culture over 12 days during which SIRV3 anti-CRISPR genes were shown to be expressed. Transcriptome and proteome analyses demonstrated that most SIRV3 genes were expressed at varying levels over time whereas SMV1 gene expression was generally low. The study yields insights into the basis for the stable infection of SIRV3 and the resistance to the different host CRISPR-Cas interference mechanisms. It also provides a rationale for the commonly observed coinfection of archaeal cells by different viruses in natural environments.

Keywords: *Sulfolobus*, archaeal viruses, carrier state infection, CRISPR-Cas adaptation and interference, Acr proteins.

1. Introduction

Viruses play important roles in nature in shaping microbial communities [1]. Many studies have been undertaken of diverse virus-prokaryote infections but they have focused mainly on those producing cell lysis or lysogens [2]. Infections producing cell lysis may eventually lead to viral loss whereas lysogenic infections impair viral multiplication by suppressing expression of most viral genes and by converting host cells to superinfection-resistant lysogens. A central question remains as to how viruses, or virus mixtures, co-exist stably within hosts in natural environments.

Carrier state infection was originally described in 1961 for bacteriophages [3] but although it has been studied periodically in bacteria almost nothing is known for archaea. Of the 100 or so archaeal viruses characterised, very few have been shown to

cause cell lysis [4] while some, in particular fuselloviruses, readily integrate into host genomes [5,6]. In addition, many are released constantly into infected cultures, at a low rate, without significantly impeding host growth [7-10].

In bacteria carrier state infection has been characterised for phages that existed episomally in a small fraction of host cells and were stably maintained without causing cell lysis [11]. Recently, single cell analyses of phage P22-infected *Salmonella* yielded insights into the mechanism involved [12]. P22 is a temperate phage able to undergo both lytic and lysogenic cycles. Before entering the lysogenic state, *Salmonella*, harbouring a polarly-tethered carrier state P22, overproduced phage-encoded immunity factors to prevent superinfection. These were inherited cytoplasmically by the P22-free daughter cells and produced transient resistance against P22. On cell division, dilution of the immunity factors conferred phage susceptibility to a subpopulation. Thus, a P22-infected *Salmonella* culture was able to exist in multiple states, lytic, lysogenic, carrier state and P22 free [12].

Here we demonstrate a carrier state infection of *S. islandicus* REY15A by SIRV3, a rudivirus closely related to SIRV2 [13] that induces cell lysis in *S. islandicus* LAL14/1 [4]. SIRV3 only infected a subpopulation of strain REY15A cells and the fraction of actively infected cells remained relatively stable over 7 generations. In order to activate host CRISPR-Cas activity against SIRV3, and to test the effect on SIRV3 maintenance, the culture was coinfected with the bicaudavirus SMV1 [14] that stimulates CRISPR-Cas spacer acquisition against coinfecting viruses or plasmids while remaining resistant itself [14-16]. We tested the viral propagation and interplay with the three different CRISPR-Cas interference systems of strain REY15A. Both viruses were stably maintained in the culture over a 12 day period but SIRV3 was expressed more actively than SMV1. Transcript levels of the viruses and host were monitored for up to 4.5 days post-infection (dpi), and viral expression levels peaked at 2.5 - 3 dpi, coincident with activation of CRISPR-Cas adaptation when SIRV3 was the primary target for CRISPR spacer acquisition. Host genes that yielded strongly enhanced transcript levels in coinfected samples encoded, in particular, subtype I-A CRISPR-Cas proteins, diverse VapBC antitoxin-toxins and transposases. Transcriptomic and proteomic analyses were undertaken on the viruses and infected cells undergoing CRISPR-Cas adaptation.

Factors influencing the infection of strain REY15A by SIRV3 are considered including a mutated cellular receptor [17] and virus-encoded anti-CRISPR proteins (Acr)

[18]. We also hypothesise on the potential benefits of viruses coinfecting host cells in natural environments.

2. Results

2.1. Genomic and proteomic features of SIRV3 and SMV1

SIRV3 was isolated from a hot spring in the Gunnuhver geothermal area of Iceland [14] and was infected in *S. islandicus* REY15A. dsDNA was extracted from virions and the genome was sequenced (Genbank accession number KX712143). The linear genome map (Figure 1) contains 32,995 bp and carries 45 ORFs which share 80-95% amino acid sequence identity with SIRV2 homologs, except for gp06 (ORF48) and gp38 (ORF90) which show ~30% sequence identity with proteins encoded by other rudiviruses [13] and gp40 (ORF149) that yielded no significant match amongst public database sequences. The genome carries characteristic rudiviral long inverted terminal repeats [13].

The circular genome of SMV1 was analysed earlier (Genbank accession number HG322870.1) and it carries 48,775 bp, 51 ORFs and three transposable elements [15] but the virion proteins remain uncharacterised. The virus exhibits an exceptional life cycle that involves extracellular tail development [19].

Proteins from the purified virions of SIRV3 and SMV1 were identified, and their abundance estimated, by mass spectrometry (Table 1). SIRV3 virions carried the major rudiviral coat protein gp19 (ORF134), a minor component gp29 (ORF1070), and very minor components gp05 (ORF131) and gp17 (ORF158) (Figure 1). Homologs of gp05 and gp17 were not detected earlier as structural proteins in SIRV2 [20].

SMV1 virions were complex with 16 major, medium and minor protein components one of which gp11 (ORF114) was characterised earlier[14] (Table 1). Some of these were homologous to virion proteins of *Acidianus* bicaudavirus ATV [21]. They included a MoxA AAA ATPase (gp24) and a von Willebrand factor domain protein (gp23). Four SMV1 virion proteins (gp09, gp23, gp34 and gp47) were homologous to ATV-encoded proteins that were not detected in virions [21].

2.2. SIRV3 undergoes carrier state infection in S. islandicus REY15A

SIRV2 induces cell lysis in *S. islandicus* strain LAL14/1 with virions extruding via pyramid-like structures formed in the cell membrane [4,22]. Therefore, SIRV3 was propagated in strains LAL14/1 and REY15A. Both hosts carry multiple CRISPR spacers

matching SIRV3 bearing zero or one or more mismatches (Table 2). The growth curves showed that whereas SIRV3 infection at MOI 1 completely inhibited growth of strain LAL14/1, only mild growth retardation occurred for strain REY15A when infected under similar conditions (Figure 2A). This suggested that only cells of the former were lysed, an inference that was reinforced by flow cytometry results which demonstrated that host DNA was heavily degraded in strain LAL14/1 but not in strain REY15A (Figure S1).

Consistent with these results, the plaque assay revealed that SIRV3 propagated at a high level in strain LAL14/1 (Figure 2B). In contrast, the virus titre in the supernatant of strain REY15A had only doubled 12 hours post infection (hpi) and required a further 36 hours to redouble (Figure 2C). Thus, SIRV3 propagated inefficiently in strain REY15A.

Next, we estimated the adsorption rates of SIRV3 to both strains. Whereas about 70% of SIRV3 virions bound to cells of strain LAL14/1 within 30 seconds, the adsorption rate for strain REY15A was significantly lower with only about 25% of virions adsorbed after 10 hrs incubation (Figure 2D). The results are consistent with SIRV3 undergoing a lytic infection in strain LAL14/1, similar to SIRV2 [4], whereas infection of strain REY15A was inefficient.

Then we estimated the cell fraction of strain REY15A carrying active SIRV3 over 84 hpi by expressing the core virus-encoded single-strand DNA binding protein gp12 using fluorescence microscopy [23,24]. Samples were taken at regular time intervals after infecting with SIRV3 at MOI 1. Cells were then fixed and subjected to immunohybridization with an antibody raised against SIRV2 gp17, a close homolog of SIRV3 gp12, as illustrated in Figure S2.

The proportion of SIRV3-infected cells in rich medium over 84 hpi fluctuated between 2% and 17% (Figure 3A). Importantly, there was no increase in the infection level with time and, given that the lytic life cycle of rudiviruses is about 12 hours [4,24,25], the results indicate that active SIRV3 was stably maintained. Consistent with this inference, the growth curves and cellular DNA contents of the SIRV3-infected cultures, showed no significant differences from those of the uninfected control culture (Figure 3B,C). In summary, stable maintenance of SIRV3, and the unimpeded growth of host cells over 4 days, supported the presence of an active viral infection in a small fraction of the culture.

2.3. Effect of SMV1 coinfection on the level of SIRV3 infection

SMV1 can activate CRISPR-Cas spacer acquisition against a coinfecting virus or conjugative plasmid but not against itself [14-16]. Therefore, since no spacer acquisition activity was detected in SIRV3-infected cells (see below), we examined the effect of SMV1 coinfection first on the level of SIRV3 in infected cells.

SMV1 infection of strain REY15A was tested at MOIs in the range 10^{-8} - 1. At MOIs 10^{-8}, 10^{-7} and 10^{-6} no growth retardation was observed over 100 hpi. Growth inhibition was first observed at MOI 10^{-5} (Figure 3B) and it was coincident with strong degradation of cellular DNA in about 80% of infected cells at 88 hpi, determined by flow cytometry (Figure 3C). Furthermore, very low amounts of extracellular virions (<10^4 PFU/ml) were detected at 16 hpi by plaque assays indicating that most of the cell culture had died without releasing virions.

Next, cultures were coinfected with SIRV3 (MOI 1) and SMV1 (MOI 10^{-5}, 10^{-6} and 10^{-7}), adding first SIRV3 and then SMV1, and the proportion of cells infected with active SIRV3 was monitored over 84 hours. At SMV1 MOIs 10^{-6} and 10^{-7}, the infection level of SIRV3 fluctuated between 0 and 14%, similar to the range of 2 - 17% observed for the culture infected with SIRV3 alone (Figure 3A). Notably, the active SIRV3 infection level (<3%) also remained low in the culture coinfected with SMV1 (MOI 10^{-5}) possibly due to cell death caused by the relatively high SMV1 MOI (Figure 3A). Repeated experiments under the same conditions (SIRV3 alone and coinfected at three different SMV1 MOIs) produced minor fluctuations at the same time points but infection levels were always less than 20% (Figure S3). It was concluded that whereas coinfection with SMV1 at low MOI did not significantly reduce the SIRV3 infection level, at higher MOIs some cell death occurred that limited viral infection.

Therefore, we infected SIRV3 at about MOI 1 and then SMV1 at MOI below 10^{-5}, and the densities of uninfected and coinfected cells were measured at A_{600} with dilutions of fresh medium every 3-4 days over 12 days. Growth retardation occurred at 2-3 dpi and it increased over 3.5-7.5 dpi. Subsequent growth recovery at 8-9 dpi preceded strong retardation at 9.5-11 dpi (Figure S4A). Viral concentrations were determined by diluting samples to the same DNA concentration and then viral genes (gp40 of SIRV3 and gp11 of SMV1) were PCR amplified and analysed by visually estimating intensities of the PCR bands (Figure S4B). The results demonstrated that SIRV3 DNA levels remained fairly constant until 9 dpi and then increased while SMV1 DNA levels were fairly constant over 12 days (Table 3).

2.4. CRISPR-Cas spacer acquisition from SIRV3 induced by SMV1

Strain REY15A carries three different CRISPR-Cas interference systems, subtype I-A, subtype III-Bα and subtype III-Bβ and a single CRISPR-Cas adaptation module [26]. Therefore next we tested whether SMV1 coinfection activated CRISPR-Cas adaptation from SIRV3. The leader-end regions of CRISPR loci 1 and 2 from SIRV3-infected and the coinfected samples were PCR amplified. The appearance of new larger PCR products in agarose gels occurred only from the coinfected sample indicating the onset of spacer acquisition in the CRISPR loci at 3-3.5 dpi (Figure S4C) and this effect coincided with growth retardation of the coinfected sample at 3-3.5 dpi (Figure S4A).

Next, we performed a transcriptome analysis of the uninfected and infected samples with the aim to determine: (a) identities of new CRISPR spacers acquired from viral DNA, and (b) transcript levels of the CRISPR-Cas machinery. Total RNA was extracted from samples taken from the same culture at time points 2, 2.5, 3, 3.5 and 4.5 dpi and from an uninfected and SIRV3-infected culture at 4 dpi carrying a very low level of virus (Table 4). Libraries were prepared and sequenced yielding in total about 123 x 10^6 paired-end 51 bp reads. Transcript sequences from each sample were aligned with the viral and host genomes (Table 4).

Transcript abundance levels of both viruses in the coinfected samples rose sharply after 2.5 dpi, albeit at about a 20-fold higher level for SIRV3 (Table 4). However, whereas the SIRV3 transcript levels peaked at 3 dpi, they remained fairly constant for SMV1 with an increase at 4.5 dpi (Table 4). SIRV3 transcript levels were very low in the SIRV3-infected sample (4 dpi) (Table 4) while the host transcript profile was closely similar to that of the uninfected sample (Table 4).

First, we examined the CRISPR leader transcripts for newly acquired spacers in each coinfected sample. An increasing fraction of transcripts (0.7% to 2.2%) carried newly acquired spacers from SIRV3, in both CRISPR loci, throughout the late infection period (Table 5).

The seven samples were then divided into three groups and a differential transcription analysis was performed. The groups reflect the observed phases of infection development: (a) an uninfected and minimally SIRV3-infected samples as control group; (b) 2 and 2.5 dpi samples represent the "early" infection phase; and (c) 3, 3.5 and 4.5 dpi samples where viral transcript levels increased and CRISPR-Cas adaptation was activate constitute the "late" infection stage. The global transcriptional profile comparison shows a clear segregation between the three groups, strongest

between the "control" and coinfected groups and with a smaller time-course difference underpinning the division between the early and late infected groups (Figure S5A).

Transcripts were detected from the CRISPR-Cas adaptation cassette and the three interference cassettes (subtypes I-A, III-Bα and III-Bß) in all samples (Table 6). However, coinfection yielded strongly increased transcript abundance in the late infection phase from the CRISPR loci, *cas1*, essential for CRISPR adaptation, and from the subtype I-A interference gene cassette (Table 6). In contrast, transcript levels from some type III-Bβ interference genes were strongly reduced (Table 6).

2.5 Cellular transcript abundance changes in coinfected samples

Significant fold changes in transcript abundance were observed for many host genes, especially in the late infection phase. In particular, transcripts from five of the 21 *vapBC* antitoxin-toxin gene pairs were significantly ($p<0.05$) enhanced (Table S2). The strong activation closely paralleled earlier observations on virus-infected *S. islandicus* strains undergoing CRISPR-Cas activity [27,28] suggesting that it is a general virus infection response in *Sulfolobus*.

Large changes in transcript abundance, mainly increases, were also observed from IS element-encoded genes, five of which corresponded to IS605-*orfB* genes, or fragments thereof, including two genes (SiRe0752 and SiRe0773) neighbouring CRISPR loci (Table S2). In contrast to the antitoxin-toxin results many of the latter changes were detected at the early infection stage (Table S2).

Transcript levels of the cell division *cdv* operon (SiRe1173-SiRe1175), and most DNA replication genes, were not altered significantly, consistent with normal host growth. In contrast, transcript abundance levels from some several transcriptional regulator genes were significantly up- or down-regulated (data not shown).

2.6. Viral proteome analysis of coinfected samples

Proteome analyses were performed on the uninfected sample and the coinfected sample undergoing CRISPR-Cas adaptation at 3.5 dpi, from the same culture as used in the transcriptome study. Approximately 70% of the total host-encoded proteins were detected (data not shown). Most SIRV3-encoded proteins yielded positive spectral counts (Table S1) and the major virion proteins gp19 and gp29 were especially abundant (Table 1). In general, protein levels for SMV1 were low, consistent with the

transcription data (Table 4), and only five SMV1 proteins were detected three of which were virion proteins (Table S1).

3. Discussion

Archaea host a wide variety of viruses exhibiting diverse morphotypes and genometypes and many of those characterised are stably maintained intracellularly alone or as mixtures [7-10]. However, little is currently known about the factors influencing this stability. Here we studied two different viruses. The rudivirus SIRV3 contains characteristic linear dsDNA genome with inverted terminal repeats and covalently linked ends [13,29] and the virions exhibit a major coat protein gp19/ORF134 [13] and three minor components (Table 1); some differences were observed in the minor protein components from those described earlier for SIRV2 [20]. SMV1 carries a circular dsDNA genome [15] and 16 virion proteins (Table 1) and is related to the bicaudavirus ATV [21]. Both viruses undergo exceptional extracellular virion tail development [14,19,21] inferred to be induced by a co-chaperone complex of a MoxA AAA-ATPase and a von Willebrand domain protein [30].

On infecting strain REY15A with SIRV3 alone, virions were adsorbed weakly to host cells relative to strain LAL14/1 and minimal cell lysis was detected. The weak adsorption may result from the occurrence of truncations in host genes encoding protein components of one putative rudiviral receptor [2,17]. SIRV3 also propagated stably in a small fraction of the cellular population and did not induce a detectable CRISPR-Cas adaptation response.

In order to test the influence of CRISPR-Cas activity on the level of SIRV3 infection, it was activated on coinfecting with SMV1 that induces spacer acquisition against coinfecting genetic elements [14,15] possibly as a result of increased cellular stress generated by two genetic elements. The specific targeting of SIRV3 may partly reflect that spacer acquisition is dependent on active viral replication [14,31] and rudiviruses produce exceptionally complex replication intermediates [23].

Spacer acquisition from SIRV3 occurred in the late infection phase of the coinfected samples coincident with enhanced transcript levels from the spacer acquisition gene *cas1* and subtype I-A interference genes (Table 6). This activity coincided with a partial decrease in the total level of SIRV3 transcripts (Table 4) but both viruses remained in the culture throughout the 12 day period (Table 3) although their transcriptional activities peaked at different times (Table 4). The transcript levels of SMV1 were lower

than those of SIRV3 overall but also showed a marked increase at 3 dpi, albeit 19-fold lower than SIRV3, with a second stronger increase at 4.5 dpi (Table 4). These results are consistent with the proteome data obtained at 3.5 dpi when most SIRV3-encoded proteins were detectable *in vivo* whereas only a few SMV1 proteins including three of the 16 virion proteins were present in low yields (Table S1).

The presence of multiple SIRV3-matching spacers in CRISPR loci of strain REY15A (Table 2), together with the new spacers added in the coinfected cultures after 3 dpi (Table 5), were expected to provide a robust viral defence [32,33]. A likely explanation for the survival of the active viruses is that CRISPR-Cas interference was inhibited by Acr proteins encoded by SIRV3. One Acr protein (gp02) was recently shown to inhibit subtype I-D CRISPR-Cas interference of strain LAL14/1, and two further SIRV3-encoded homologs (gp36 and gp37) were predicted to perform anti-CRISPR functions [18]; moreover, all three proteins were expressed in the coinfected cells (Table S1).

The latter hypothesis is strengthened by a recent study of strain REY15A infection with SMV1 alone [34]. Guo et al. demonstrated that SMV1 was susceptible to attack from type IIIB but not the subtype I-A interference complex, where the former degrades RNA and DNA and the latter dsDNA [34]. They inferred that the virus encoded an Acr protein specific for the latter subtype I-A complex. Potentially, that could, have protected DNA of both SMV1 and SIRV3 from degradation in our coinfected samples, despite the strongly increased transcript levels observed for the subtype I-A interference proteins (Table 6). Furthermore, the observation that transcript yields from the type IIIB interference genes were strongly reduced in the coinfected samples (Table 6) suggests that a second mechanism was activated to repress the latter immune system. The susceptibility of SMV1 to type IIIB interference also provides an explanation for the low levels of SMV1 transcripts observed in our coinfected cultures because they would be a target for type IIIB interference.

In conclusion, we show that SIRV3 undergoes a carrier state infection in strain REY15A whereby active virus is maintained in a low fraction of cells over longer periods. The presence of the second co-infecting virus SMV1 appeared to facilitate the stability of this state, despite the activation of the CRISPR-Cas immune response. This suggests that there is an ongoing, and unresolved, conflict between virus and host that is affected by inefficient cell entry of SIRV3 and specific blockage of the CRISPR-Cas interference complexes by Acr proteins with different specificities and potentially from both viruses. Thus, a likely explanation for the stable coinfection observed here, and for

the similar coinfections frequently observed in natural thermophilic environments, is that the coinfecting viruses complement one another by providing Acr proteins which target the different types of CRISPR-Cas interference encoded by the host.

4. Materials and methods

4.1. Sulfolobus *cultures and nucleic acid preparation*

S. islandicus REY15A was cultured in *Sulfolobus* medium supplemented with 0.2% trypton, 0.1% yeast extract and 0.2% sucrose (TYS medium) at 78ºC. The rudivirus SIRV3 and monocaudavirus SMV1 were propagated and isolated as described [14,35]. The viruses were coinfected into *Sulfolobus* cultures and cell densities were monitored at A_{600} in 50 mL batches and diluted to A_{600} = 0.05 with fresh medium in every 3-4 days when uninfected control cultures exceeded A_{600} = 1 in order to prevent cell death from nutrient deficiency. Samples were taken every 24 hr and cells were harvested by centrifugation (6000 g, 10 min). SIRV3 infection was detected by PCR amplifying gp40 (ORF149) using primers forward 5'-CTAATAAGACAAGAACATCAG-3' and reverse 5'-CATATATAGTATTGGTGAAAAG-3'; SMV1 infection was detected by PCR amplifying gp11 (ORF153) using primers forward 5'-GCGGATTCGCCCCTGCAGGTACG-3' and reverse 5'-GTCTCTCTCATATTTGCAATC-3'

DNA was isolated using DNeasy Blood & Tissue Kit (Qiagen, Hilden, Germany) and sequencing of the SIRV3 DNA was performed by GATC Biotech (Konstanz, Germany) and the genome was assembled using the with CLC genomics workbench (Qiagen). Total RNA was extracted using the TRIzol reagent (Sigma Aldrich, Copenhagen, Denmark) following the manufacturer's protocol.

4.2. Plaque assay

Approximate virus titres (PFU/ml) were determined by plaque assays after purification, infection and coinfection. Serial dilutions (10.0 µL) of viral preparations were mixed with 2.0 mL of exponentially growing host culture (2 x 10^8 cells); *S. islandicus* ΔCRISPR_1 LAL14/1 for SIRV3 infection[35] and *S. islandicus* ΔC1C2 for SMV1 infection [36]. The mixture was incubated for 30 min at 78°C to allow for adsorption of viruses onto host cells. Immediately after adding 1 mL of 0.4% (w/v) Gelrite (78%) or 2 mL of 0.4% (w/v) Gelrite (78%) for SIRV3 and SMV1 mixtures, respectively, the sample was layered on a premade 0.7% (w/v) Gelrite plate (78°C). Plates were incubated for 2-3 days at 78°C. SIRV3 plaques were small and turbid

whereas SMV1 plaques appeared as small clear halozones. Single plaques were counted and PFU values were determined.

4.3. Determination of SIRV3 burst size and adsorption rate

The SIRV3 burst size in strain REY15A was measured according to Bize et al. [4]. Briefly, REY15A cells were infected with SIRV3 at MOI 0.1 and the virus titer (PFU/ml) in the supernatant at 12 hpi was measured by the plaque assay. The cell density was estimated as 10^8 cells/ml at A_{600} 0.15. The burst size was estimated by dividing the virus titer at 12 hpi with the cell density. SIRV3 adsorption rates in strains REY15A and LAL14/1 were determined as described by Uldahl et al. [19]. The cells were infected with the virus at MOI 1 and the virus titer (PFU/ml) in the supernatant, i.e. the virus remaining unadsorbed at 30 seconds post-infection, was determined by the plaque assay. The level of viruses adsorbed to cells was estimated relative to the amount initially added.

4.4. Flow cytometry analysis

Strain REY15A cells were infected with SIRV3 (MOI ≈ 1) and SMV1 (MOI variable) with samples taken at regular intervals from uninfected, single infected and coinfected cultures. 300 µl culture was mixed with 700 µl of 100% ethanol and stored at 4°C. After all samples were collected, the fixed cells were centrifuged at 8000 rpm for 4 min and resuspended in 1 ml of 10 mM Tris-HCl (pH 7.5), 10 mM $MgCl_2$. Samples were recentrifuged under the same conditions and pellets were resuspended in 150 µl fresh staining solution containing ethidium bromide (20 µg/ml) and mithramycin (100 µg/ml) for 1 hr. Samples were kept cold at all steps and analyzed in an ApogeeFlow A-40 flow cytometer illuminating with a 405 nm laser (Apogee Flow Systems, Hemel Hempstead, UK). Statistical analyses of the qualitative flow cytometry results were performed by using Flowing Software 2 [http://flowingsoftware.btk.fi].

4.5. Immunofluorescence staining

Cells recovered by centrifugation at 8000 rpm for 3 min. were fixed by suspending in 4% paraformaldehyde for 10 min at room temperature. They were washed three times with PBS buffer (10 mM Na_2HPO_4, 2 mM KH_2PO_4, pH 7.4, 137 mM NaCl, 2.7 mM KCl) and were pelleted at 8000 rpm for 3 min and resuspended in PBS. Samples were permeabilized with PBS + 0.1% Tween®20 (PBST) for 15 min at room temperature and

washed three times with PBS. 10 µl cell-suspension was spotted onto poly-L-lysine-coated slides (Sigma-Aldrich) and air-dried. Slides were rinsed with PBS and incubated with PBST + 1% bovine serum albumin (BSA) for 15 min at room temperature. Thereafter, slides were incubated with the corresponding primary antibody diluted in PBST + 1% BSA for 1 hr at room temperature. Guinea rabbit anti-gp17 polyclonal antibody was used at a dilution of 1:5000. After three washes of 2 min each with PBS, the slides were incubated with the corresponding secondary antibody diluted in PBST + 1% BSA for 1 hr at room temperature. The commercial secondary antibody Alexa Fluor® 488 goat anti-guinea rabbit was used at a dilution of 1:1000. Slides were washed three times with PBS and incubated with 10 µM 4', 6-diamino-2-phenylindole (DAPI) (Sigma-Aldrich) for 5 min at room temperature and then washed a further three times with PBS and mounted with PVP mounting medium (1x PBS, 78% glycerol and 0.2% polyvinyl pyrrolidone). Finally, slides were analyzed using a Nikon Eclipse Ti-E inverted microscope coupled to an Andor Zyla 5.5 sCMOS camera. Images were processed using Adobe Photoshop CS6.

4.6. Transcriptome analysis

Paired-end HiSeq reads were analysed for 7 libraries including one uninfected control culture, another infected with a low level of SIRV3 and five samples of coinfected with SIRV3 and SMV1 taken at times 2, 2.5, 3, 3.5 and 4.5 dpi. Total RNA libraries were constructed from each sample and 51 bp from each end was sequenced in an Illumina HiSeq 2500 at GATC Biotech AG (Konstanz, Germany). All reads were mapped independently on the viral and host genomes strain REY15A (CP002425), SIRV3 (KX712143) and SMV1 (NC_023585) using ERANGE within the CLC Genomics Workbench (CLC Bio, version 7.0, Qiagen) [37]. Default settings for the algorithm for sequence matching were: mismatch cost 2, gap opening and extension costs 3, minimal alignment/similarity region 80%. Total numbers of transcripts were used for differential host transcription analysis using EdgeR version 3.16.5 [38]. General transcriptional profiles were compared before the differential analyses to verify that sample groups were clustering together and thus coherent (Figure S5). Three groups were compared pairwise: a control group including uninfected or minimally SIRV3 infected libraries (n=2), an early coinfection group including 2 and 2.5 dpi samples (n=2), and a late infection group comprising the 3, 3.5 and 4.5 dpi samples (n=3). Genes were considered differentially transcribed below a false discovery rate (FDR)-corrected p-

value of 0.05 [39]. For the analysis the total transcript counts for each gene were employed after excluding rRNA and ncRNAs reads (counts per million). In order to remove noise from low-transcription genes, only those with >1 count per million in 5 or more libraries (from a total of 7) were retained for the analysis.

4.7 Quantifying new spacer acquisition

CRISPR spacer acquisition was monitored over an 8 day period by PCR amplifying leader-proximal regions of both CRISPR loci using 5'-GTCCATAGGAG GACCAGCTTTC-3' and 5'-CCAACCCCTTAGTTCCTCCTCTATAG-3' for locus 1, and 5'- GTTCCTTCCACTATGGGACTAGGAAC-3' and 5'-CGTCACTGACACCATATTTATAC-3' for locus 2. PCR products were resolved in 1% agarose gels and detected by ethidium bromide staining under UV light (Doc-ItLS; UVP, Cambridge, UK).

CRISPR RNA reads were collected by selecting records containing a 36 nt sequence corresponding to the full repeat sequence CTTTCAATTCTATAGTAGATTAGC, using the Biopieces bioinformatics toolset (www.biopieces.org). New CRISPR spacers and their protospacer origins were identified by BLAST alignments to a local database of the host and viral genomes using word size 28 nt for spacer sequences, mismatch cost 3 and gap cost 2. The overall level of CRISPR adaptation activity was estimated from the proportion of transcripts carrying *de novo* virus-matching spacers relative to the number of wild-type leader-end transcripts in each sample. The protospacer origin of the de novo CRISPR spacers was analyzed using BLAST. Only forward reads of each library insert were used for quantification.

4.8. Proteome analysis

Virus particles were purified by CsCl density gradient as described earlier [40]. For mass spectrometric analysis, proteins were in-gel-digested with trypsin as described previously [41]. Extracted peptides were analyzed by liquid chromatography tandem mass spectrometry (LC-MS/MS) on an Orbitrap XL instrument (Thermo Fisher Scientific) under standard conditions. Peptide fragment spectra were searched against open reading frames of SIRV3 and SMV1. The proteome data were analysed with the MaxQuant package which yielded peptide counts, sequence coverage, total spectral counts, intensity and PEP score values [42]. The data obtained for proteins isolated from SIRV3 and SMV1 were analysed against a database comprising only virus

proteins, whereas results obtained for the host, and infected host, proteins were analysed against a database for all host and viral proteins.

Acknowledgements

M. Raabe and U. Pleßmann are thanked for technical assistance with the proteomics analysis

Funding

The work was supported by Danish Council for Independent Research/Technology and Production (grant number DFF–7017-00060) to XP and by grants from Copenhagen University to SE, CL-S and RAG. The proteomics analysis was supported by the Deutsche Forschungsgemeinschaft (DFG - FOR 1680).

References

1. Suttle A. Viruses - major players in the global ecosystem. Nat Rev Microbiol 2007;5(10):801-812.
2. Hobbs Z, Abedon ST. Diversity of phage infection types and associated terminology with “Lytic or lysogenic” FEMS Microbiol Lett 2016;363(7):pii:fnw047.
3. Li K, Barksdale L, Garmise LJ. Phenotypic alterations associated within the bacteriophage carrier state of *Shigella dysenteriae*. Gen Microbiol 1961;24:355-367.
4. Bize A, Karlsson EA, Ekefjärd K, et al. A unique virus release mechanism in the Archaea. Proc Natl Acad Sci USA 2009;106:11306-11.
5. Reiter WD, Palm P, Yeats S. Transfer RNA genes frequently serve as integration sites for prokaryotic genetic elements. Nucleic Acids Res 1989;17(5):1907-14.
6. Wiedenheft B, Stedman K, Roberto F, et al. Comparative genomic analysis of hyperthermophilic archaeal f*uselloviridae* viruses. J Virol 2004;78:1954–1961.
7. Zillig W, Arnold HP, Holz I, et al. Genetic elements in the extremely thermophilic archaeon *Sulfolobus*. Extremophiles 1998;2:131-140.
8. Prangishvili D, Forterre P, Garrett, RA. Viruses of the Archaea: a unifying view. Nat Rev Microbiol 2006;4:837–848.
9. Pina M, Bize A, Forterre P, et al. The archeoviruses. *FEMS Microbiol Rev* 2011;35: 1035-1054.
10. Wang H, Pen, N, Shah SA, et al. Archaeal chromosomal elements. Microbiol Mol Biol Rev 2015;79(1):117-152.

11. Siringan P, Connerton PL, Cummings NJ, et al. Alternative bacteriophage life cycles: the carrier state of *Campylobacter jejuni*. Open Biol 2014;4:130200.
12. Cenens W, Makumi A, Govers SK, et al. Viral transmission dynamics at single-cell resolution reveal transiently immune subpopulations caused by a carrier state association. PLoS Genet 2015;11(12):e1005770.
13. Peng X, Blum H, She Q, et al. Sequences and replication of the archaeal rudiviruses SIRV1 and SIRV2: relationships to the archaeal lipothrixvirus SIFV and some eukaryal viruses. Virology 2001;291:226-234.
14. Erdmann S, Le Moine Bauer S, Garrett RA. Inter-viral conflicts that exploit host CRISPR immune systems of *Sulfolobus*. Mol Microbiol 2014;91:900–917.
15. Erdmann S, Shah SA, Garrett RA. SMV1 virus-induced CRISPR spacer acquisition from the conjugative plasmid pMGB1 in *Sulfolobus solfataricus* P2. Biochem Soc Trans 2013;41:1449–1458.
16. Erdmann S, Garrett RA. Selective and hyperactive uptake of foreign DNA by adaptive immune systems of an archaeon via two distinct mechanisms. Mol Microbiol 2012;85:1044–1056. Corrigendum Mol Microbiol 2012;86:757.
17. Deng L, He F, Bhoobalan_Chitty Y et al. Unveiling cell surface and type IV secretion proteins responsible for archaeal rudivirus entry. J Virol 2014;88(17):10264-8.
18. He F, Bhoobalan-Chitty Y, Van LB, et al. Anti-CRISPR proteins against a type I-D CRISPR-Cas immunity encoded by archaeal lytic viruses. Nat Microbiol 2018;3(4):461-469.
19. Uldahl KB, Jensen SB, Bhoobalan-Chitty Y, et al. Life cycle characterization of *Sulfolobus* monocaudavirus 1, an extremophilic spindle-shaped virus with extracellular tail development. J Virol 2016;90:5693-5699.
20. Vestergaard G, Shah SA, Bize A, et al. *Stygiolobus* rod-shaped virus and the interplay of crenarchaeal rudiviruses with the CRISPR antiviral system. J Bacteriol 2008;190(20):6837-45.
21. Prangishvili D, Vestergaard G, Häring M, et al. Structural and genomic properties of the hyperthermophilic archaeal virus ATV with an extracellular stage of the reproductive cycle. J Mol Biol 2006;359:1203-1216.
22. Brumfield SK, Ortmann AC, Ruigrok V, et al. Particle assembly and ultrastructural features associated with replication of the lytic archaeal virus *Sulfolobus* turreted icosahedral virus. J. Virol 2009;8:5964-70.

23. Martinez-Alvarez L, Bell SD, Peng X. Multiple consecutive initiation of replication producing novel brush-like intermediates at the termini of linear viral dsDNA genomes with hairpin ends. Nucleic Acids Res 2016;44(18):8799-8809.
24. Martinez-Alvarez L, Deng L, Peng X. Formation of a viral replication focus in *Sulfolobus* cells infected by the rudivirus *Sulfolobus islandicus* rod-shaped virus 2. J Virol 2017;91(13): e00486-17.
25. Okutan E, Deng L, Mirlashari S, et al. Novel insights into gene regulation of the rudivirus SIRV2 infecting *Sulfolobus* cells. RNA Biol 2013;10(5):875-85.
26. Vestergaard G, Garrett RA, Shah SA. CRISPR adaptive immune systems of Archaea. RNA Biol 2014;11:156–167.
27. León-Sobrino C, Kot WP, Garrett RA. Transcriptome changes in STSV2-infected *Sulfolobus islandicus* REY15A undergoing continuous CRISPR spacer acquisition. Mol Microbiol 2016;99:719-728.
28. Quax TEF, Voet M, Sismeiro O, et al. Massive activation of archaeal defense genes during viral infection. J Virol 2013;87:8419–8428.
29. Bautista MA, Black, JA, Youngblut ND, et al. Differentiation and structure in *Sulfolobus islandicus* rod-shaped virus populations. Viruses. 2017;9(5):pii:E120.
30. Scheele U, Erdmann E, Ungewickell EJ, et al. Chaperone role for proteins p618 and p892 in the extracellular tail development of *Acidianus* two-tailed virus. J Virol 2011;85:4812-4821.
31. Levy A, Goren MG, Yosef I, et al. CRISPR adaptation biases explain preference for acquisition of foreign DNA. Nature 2015;520:505–510.
32. Manica A, Zebec Z, Steinkellner J, et al. Unexpectedly broad target recognition of the CRISPR-mediated virus defence system in the archaeon *Sulfolobus solfataricus*. Nucleic Acids Res 2013;41:10509-17
33. Mousaei M, Deng L, She Q, et al. Major and minor cRNA annealing sites facilitate low stringency DNA protospacer binding prior to Type I-A CRISPR-Cas interference in *Sulfolobus*. RNA Biol 2016;13(11):1166-1173.
34. Guo T, Han W, She Q. Tolerance of *Sulfolobus* SMV1 virus to the immunity of I-A and III-B CRISPR-Cas systems in *Sulfolobus islandicus*. RNA Biol 2018; DOI: 10.1080/15476286.2018.1460993.
35. Gudbergsdottir S, Deng L, Chen Z, et al. Dynamic properties of the *Sulfolobus* CRISPR/Cas and CRISPR/Cmr systems when challenged with vector-borne viral and plasmid genes and protospacers. Mol Microbiol 2011;79(1):35-49.

36. Erdmann S, Garrett RA. Archaeal viruses of the Sulfolobales: Isolation, infection and CRISPR spacer acquisition. In CRISPR: Methods and Protocols (Lundgren M. et al. eds.), Methods Mol Biol 2015;1311:223-232.
37. Mortazavi A, Williams BA, McCue K, et al. Mapping and quantifying mammalian transcriptomes by RNA-Seq. Nat Methods 2008;5:621–628.
38. Robinson MD, McCarthy DJ, Smyth GK. EdgeR: a bioconductor package for differential expression analysis of digital gene expression data. Bioinformatics 2010;26:139–40.
39. Benjamini Y, Hochberg Y. (1995) Controlling the false discovery rate: a practical and powerful approach to multiple testing. J R Stat Soc Ser B Methodol 1995;57:289–300.
40. Erdmann S, Chen B, Huang X, et al. A novel single-tailed fusiform *Sulfolobus* virus STSV2 infecting model *Sulfolobus* species. Extremophiles 2014;18:51-60.
41. Shevchenko A, Wilm M, Vorm O, et al. Mass spectrometric sequencing of proteins silver-stained polyacrylamide gels. Anal Chem 1996;68:850-858.
42. Schaab C, Geiger T, Stoehr G, et al. Analysis of high accuracy quantitative proteomics data in the MaxQB database. Mol Cell Proteom 2012;11:M111.014068.

Tables

Table 1. Mass spectroscopy analyses of the protein contents of purified virions of SIRV3 and SMV1. The proteins are ordered according to decreasing spectral count values. Intracellular spectral counts from the coinfected sample at 3.5 dpi are given for comparison. nd - not detected. SMV1 genome accession number - HG322870.1.

gene product	ORF size	accession number	kDa	spectral counts	intracellular spectral counts	homologs conserved domains
SIRV3						
gp19	134	AOG61579.1	14	3160	100	coat protein
gp29	1070	AOG61587.1	124	67	264	coiled-coil
gp17	158	AOG61577.1	18	8	12	dUTPase
gp05	131	AOG61565.1	15	3	3	-
SMV1						
gp09	2028	CDF81336.1	224	3160	15	ATV-1940 WD40 domain
gp05	752	CDF81332.1	86	1929	11	transmembrane domain
gp24	588	CDF81351.1	66	1889	nd	ATV-618 MoxA ATPase
gp11	153,133, 114	CDF81338.1	≤17	711	2	ATV-131
gp06	122	CDF81333.1	14	625	2	ATV-145
gp23	759	CDF81350.1	84	499	nd	ATV-892 VWA domain
gp17	105	CDF81344.1	12	110	3	SWIM domain
gp16	156	CDF81343.1	18	157	nd	YidB-like domain
gp13	442	CDF81340.1	45	62	nd	
gp47	307	CDF81374.1	36	46	nd	ATV-286
gp32	95	CDF81359.1	11	34	2	
gp03	157	CDF81330.1	16	25	nd	transmembrane domain
gp34	242	CDF81361.1	28	24	nd	ATV-241 integrase
gp50	106	CDF81377.1	12	9	nd	RHH domain
gp19	145	CDF81346.1	16	4	nd	
gp39	292	CDF81366.1	34	0/2	nd	

Table 2. Strain REY15A CRISPR spacers showing perfect, or near perfect, base pairing matches to the SIRV3 and SMV1 genomes. The sequence corresponding to spacer 2_115 is duplicated at the termini of the SIRV3 genome. CRISPR spacer 1_83 denotes spacer 83 of CRISPR locus 1. SIRV3-matching spacers also exist in the strain LAL14/1 genome with 0 mismatches (1 spacer), 1 mismatch (4 spacers) and two and three mismatches (2 of each).

virus	CRISPR locus_spacer	base pair mismatch	protospacer location
SIRV3	1_83	0	15953-15914
“	2_115	0	255-293/32741-32703
“	2_66	1	24473-24513
“	2_100	1	21721-21761
“	1_84	2	8088-8050
“	2_45	2	18398-18437
SMV1	2_87	1	25475-25514

Table 3. Relative viral DNA levels of coinfected strain REY15A, estimated quallitiatively over 1 - 12 dpi by PCR band intensities. The relative levels are only valid for the comparison between different time points for the same virus, not for the comparison between SIRV3 and SMV1 DNA. The band intensities were estimated visually as indicated in Figure S3B.

dpi	1	2	2.5	3	3.5	4	5	5.5	6	7	7.5	8	8.5	9	9.5	10	10.5	11	12
SIRV3	+	+	+	+	+	+	+	+	+	+	+	+	+	+	++	++	++	++	++
SMV1	-	++	++	++	++	++	++	++	++	++	++	++	++	++	+	++	++	++	++

Table 4. Total host and viral transcript yields. Total numbers of transcript reads after subtracting rRNA reads are given with the percentage of reads matching host and viral genomes.

sample	dpi	total reads	SiRe (%)	SIRV3 (%)	SMV1 (%)
uninfected	5	10,520,901	100	0	0
SIRV3	4	12,241,903	99.90	0.10	0
SIRV3 + SMV1	2	14,132,316	99.74	0.22	0.04
	2.5	12,883,680	99.55	0.35	0.10
	3	53,000,092	84.38	14.85	0.77
	3.5	17,546,875	92.01	7.10	0.89
	4.5	14,433,285	89.63	4.75	5.62

Table 5. Total numbers of newly acquired SIRV3 CRISPR spacers detected amongst total leader-end transcript reads for all samples. The percentage of CRISPR transcript reads carrying new spacer sequences is given in parentheses.

virus	dpi	CRISPR leader-end reads	new SIRV3 spacers
none	5	133	0
SIRV3	4	128	0
SIRV3 + SMV1	2	984	2 (0.2%)
	2.5	592	0
	3	13224	89 (0.7%)
	3.5	766	9 (1.2%)
	4.5	820	18 (2.2%)

Table 6. Transcript level changes of host CRISPR loci and *cas* genes of the type IA CRISPR-Cas system of strain REY15A during coinfection. log_2 fold-changes are shown in the early and late infection stages relative to the control samples, and to one another. Standard *Sulfolobus cas* gene annotations are employed [23].

host gene ID	***cas/cmr* genes**	**amino acids**	**log_2 fold changes**		
spacer acquisition			early	late	late/early
SiRe_0761	*cas1*	290		+ 3.4	
I-A interference					
SiRe_0769	*cas3'*	501		+ 2.7	+ 1.9
SiRe_0770	*cas3''*	236		+ 2.5	+ 2.1
SiRe_0768	*cas5*	240		+ 3.1	+ 2.0
SiRe_0772	*cas6*	298		+ 2.7	+ 2.1
SiRe_0767	*cas7*	321		+ 2.4	
SiRe_0771	*cas8'*	345		+ 2.8	+ 2.0
SiRe_0766	*cas8''*	143	+ 1.6	+ 2.9	
III-B Cmr-β interference					
SiRe_0602	*cmr4*	286		- 1.2	
SiRe_0601	*cmr5*	155	- 1.7	- 1.2	
SiRe_0599	*cmr6*	283	- 1.4	- 1.1	
CRISPR-115 locus 1				+ 3.2	
CRISPR-93 locus 2				+ 2.3	

Figure legends

Figure 1. Genome map of SIRV3. Genes encoding virion proteins are coloured yellow and those encoding Acr proteins are green. gp02 encodes the AcrID1 that inhibits CRISPR-Cas subtype I-D activity [18]. The predicted Acr proteins gp36 and gp37 are marked.

Figure 2. A. Growth curves of strains REY15A and LAL14/1 uninfected and infected with SIRV3. B. Virus titer in the supernatant of SIRV3-infected strain LAL14/1. C. Virus titer in the supernatant of SIRV3-infected strain REY15A. D. Unadsorbed virions of SIRV3 over time in cultures of strains REY15A and LAL14/1. Data were generated from duplicate experiments and error bars indicate standard deviations.

Figure 3. Characterization of strain REY15A cells infected by active SIRV3 (MOI 1) and SMV1 (MOIs in brackets), separately and together. A. Percentage of cells infected by SIRV3 alone, or coinfected at increasing levels of SMV1. B. Growth curves of REY15A cells infected with SIRV3 or coinfected. C. DNA content of strain REY15A cells infected by the single viruses or the mixture and analysed by flow cytometry. hpi - hrs post infection. A duplicated dataset is presented in Figure S3.

Figure 1

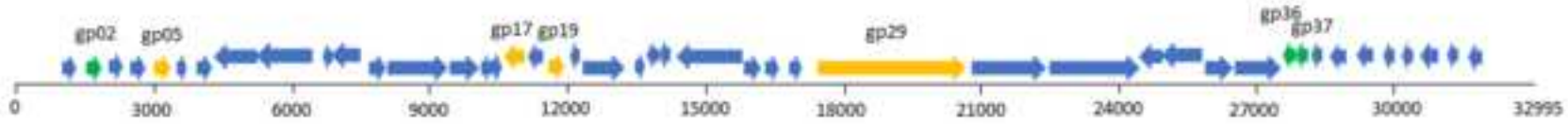
gp02
gp05
gp17
gp19
gp29
gp36
gp37
0
3000
6000
9000
12000
15000
18000
21000
24000
27000
30000
32995

Figure 2

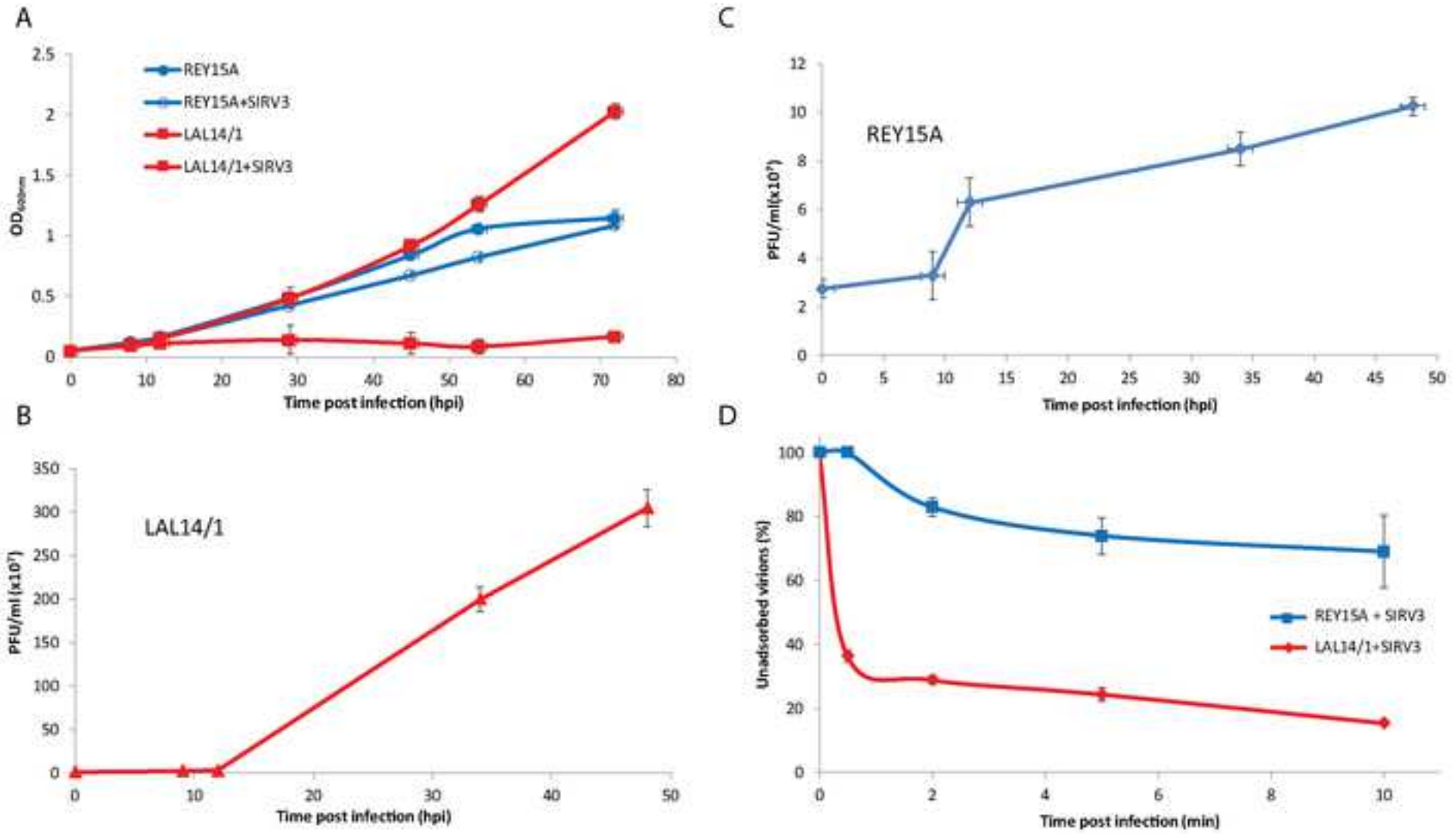
A
REY15A
REY15A+SIRV3
LAL14/1
LAL14/1+SIRV3
OD600nm
Time post infection (hpi)
B
LAL14/1
PFU/ml (x10⁷)
Time post infection (hpi)
C
REY15A
PFU/ml(x10⁷)
Time post infection (hpi)
D
Unadsorbed virions (%)
REY15A + SIRV3
LAL14/1+SIRV3
Time post infection (min)

Figure 3

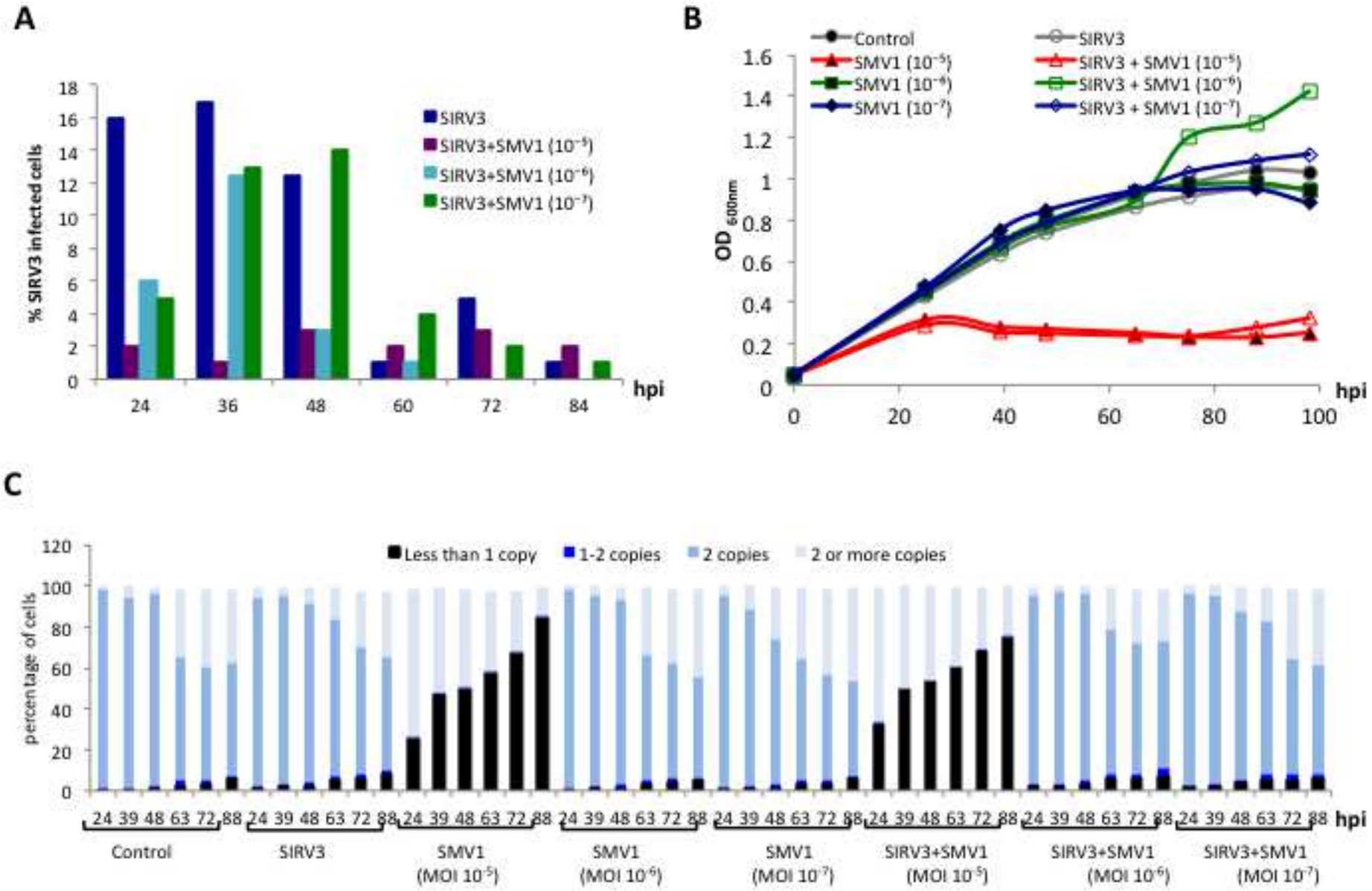
A
% SIRV3 infected cells
SIRV3
SIRV3+SMV1 (10⁻⁵)
SIRV3+SMV1 (10⁻⁶)
SIRV3+SMV1 (10⁻⁷)
hpi
B
Control
SMV1 (10⁻⁵)
SMV1 (10⁻⁶)
SMV1 (10⁻⁷)
SIRV3
SIRV3 + SMV1 (10⁻⁵)
SIRV3 + SMV1 (10⁻⁶)
SIRV3 + SMV1 (10⁻⁷)
OD 600nm
hpi
C
Less than 1 copy
1-2 copies
2 copies
2 or more copies
percentage of cells
24 39 48 63 72 88
hpi
Control
SIRV3
SMV1 (MOI 10⁻⁵)
SMV1 (MOI 10⁻⁶)
SMV1 (MOI 10⁻⁷)
SIRV3+SMV1 (MOI 10⁻⁵)
SIRV3+SMV1 (MOI 10⁻⁶)
SIRV3+SMV1 (MOI 10⁻⁷)

Supplementary Materials

Tables

Table S1. Mass spectrometry spectral count estimates of SIRV3 and SMV1 gene products in cell extracts of coinfected strain REY14A at 3.5 dpi. Acr - anti CRISPR protein homologs; vp - virion protein. gpx denotes a non annotated ORF.

gene product	kDa	spectral counts	gene product	kDa	spectral counts	gene product	kDa	spectral counts
SIRV3								
gp01	6	6	gp16	7	7	gp29_vp	124	264
gp02_Acr	11	24	gp17_vp	18	12	gp30	63	2
gp03	13	80	gp19_vp	14	100	gp31	72	13
gp04	14	1	gp20	6	2	gp32	19	6
gp05_vp	15	3	gp21	39	102	gp33	30	4
gp07	13	14	gp22	8	4	gp34	21	6
gp08	37	1	gp23	9	2	gp35	42	23
gp09	46	50	gp24	13	14	gp36_Acr	11	12
gp10	7	23	gp25	55	2	gp37_Acr	12	10
gp12	15	77	gp26	18	27	gp39	13	4
gp13	51	21	gp27	14	2	gp40	17	21
gp14	25	2	gpx	8	28	gp41	11	35
gp15	9	22	gp28	13	24	gp43	12	7
SMV1								
gp05_vp	86	11	gp11_vp	17	3	gp46	31	nd
gp06_vp	14	2	gp32_vp	11	2			
gp09_vp	224	15	gp36	12	5			

Table S2 Altered expression of antitoxin-toxin gene pairs and IS element ORFs in coinfected strain REY15A at early and late infection stages. + increased and - reduced transcript levels by ≥ 2-fold.

host gene ID	amino acids	Orf	early	late	late/early
			log_2 fold changes		
antitoxin-toxins					
SiRe_0374	80	VapB		+ 2,0	+ 2,8
SiRe_0373	131	VapC			+ 1,6
SiRe_0403	73	VapB		+ 2,0	
SiRe_0402	120	VapC		+ 2.0	
SiRe_0743	81	VapB		+ 1,7	
SiRe_0744	137	VapC		+ 1,9	
SiRe_0888	76	VapB		+ 3,4	
SiRe_2170	73	VapB		+ 1,6	+ 1,5
SiRe_2171	134	VapC		+ 1,6	
SiRe_0458	144	HEPN-domain protein		+ 2,0	
IS elements					
SiRe_0690	401	IS605_OrfB-TpnB	+ 1,6		
SiRe_0692	401	IS200/IS605_OrfB		- 3,2	- 2,7
SiRe_2602	401	IS605_OrfB-TpnB		+ 2,8	
SiRe_0752	92	IS605_OrfB-TpnB	+ 2,7	+ 2.0	
SiRe_0773	63	IS605_OrfB-TpnB		+ 3,0	
SiRe_0856	277	IS110_transposase		+ 1,8	
SiRe_0858	109	IS6_transposase	+ 4,5	+ 3,1	
SiRe_2529	164	IS6_transposase		+ 7,8	
SiRe_2432	249	IS607_transposase		+ 2,8	
SiRe_0449	275	ISC1395_Orf1	+ 2,1	+ 2,4	
SiRe_0463	236	ISC1395 _Orf2	+ 3,4	+ 3,1	

Figure Legends

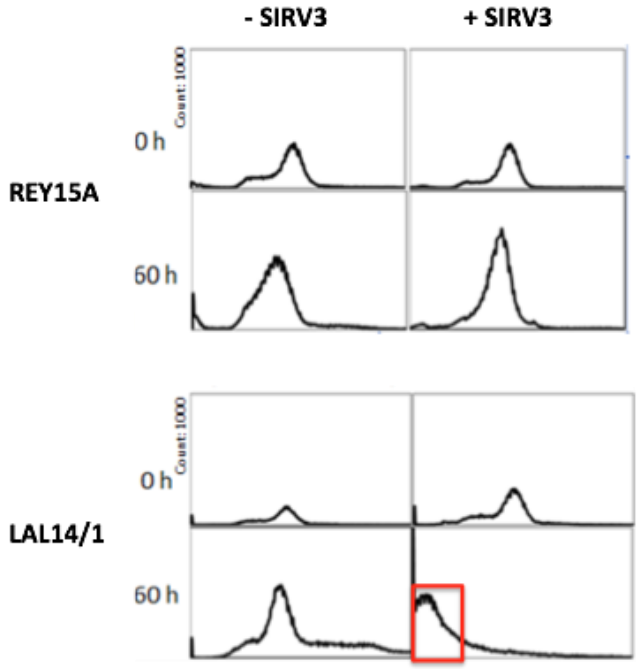

Figure S1. Cellular DNA content of cells that were uninfected (- SIRV3) or infected with SIRV3 (+ SIRV3) in strains REY15A (top) and LAL14I1 (below) The portion of DNA-less cells detected at 60 hpi in LAL14/1 cells is enclosed by the red rectangle.

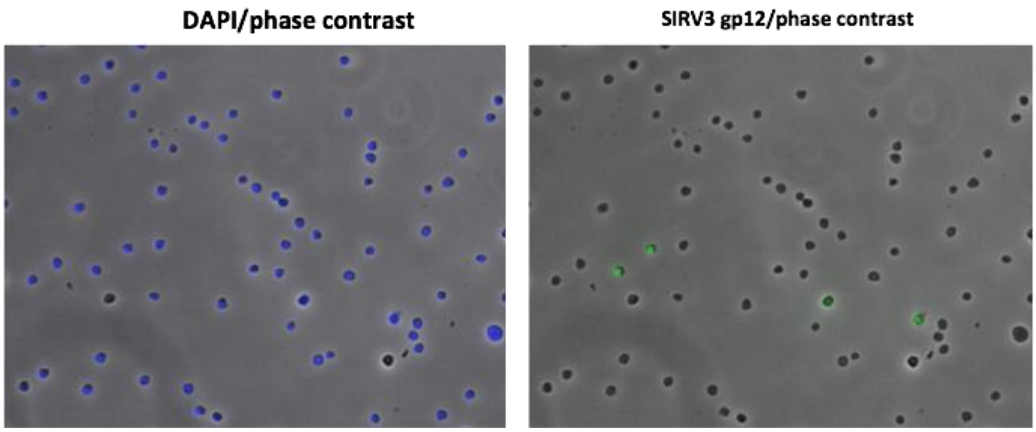

Figure S2. Immunofluorescence microscopy of SIRV3-infected REY15A cells. Left: merging of DNA stained with DAPI (blue) and phase contrast. Right: merging of SIRV3 gp12 staining (green) with phase contrast. The fraction of uninfected cells (Figure 3A) was measured by comparing the number of gp12 positive cells with those of DAPI-stained cells. Approximately 500 cells were analysed per sample.

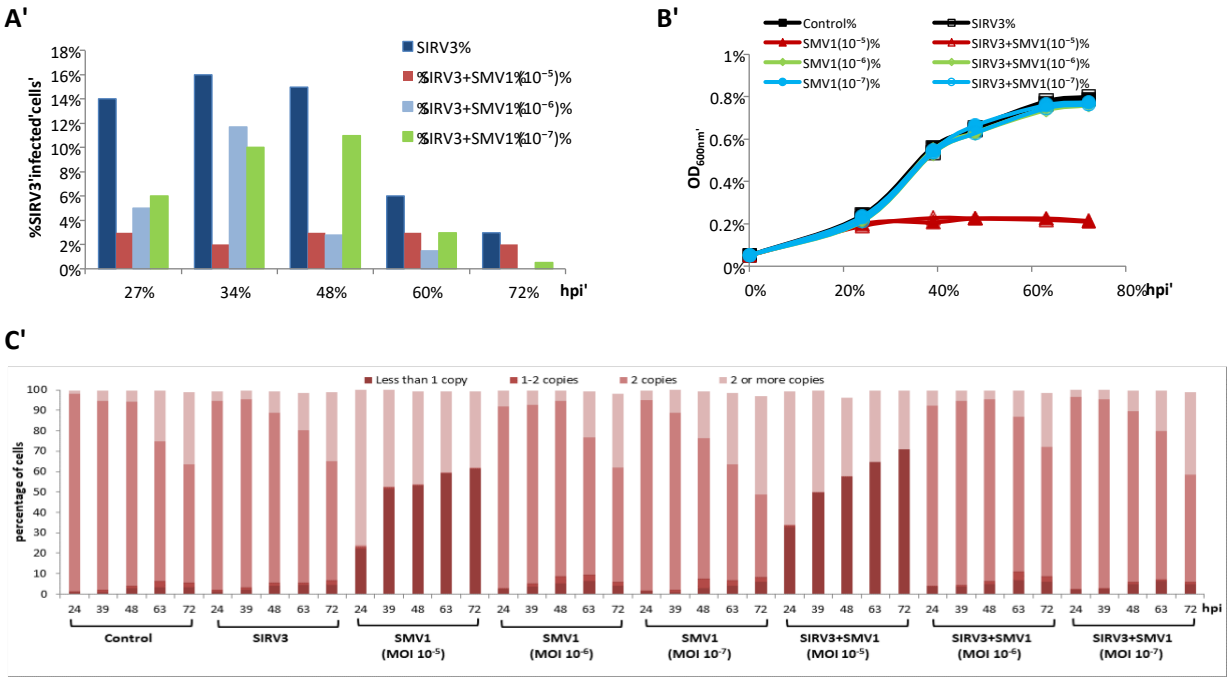

Figure S3. A second dataset for for strain REY15A cells infected by SIRV3 (MOI = 1 always) and SMV1 (MOIs in brackets), singly and together. A. Percentage of SIRV3-containing cells infected by SIRV3 alone, or by both viruses at increasing levels of SMV1. B. Growth curves of strain REY15A cells infected with SIRV3 or coinfected. C. DNA content of strain REY15A cells infected by single viruses, or the mixture, analysed by flow cytometry.

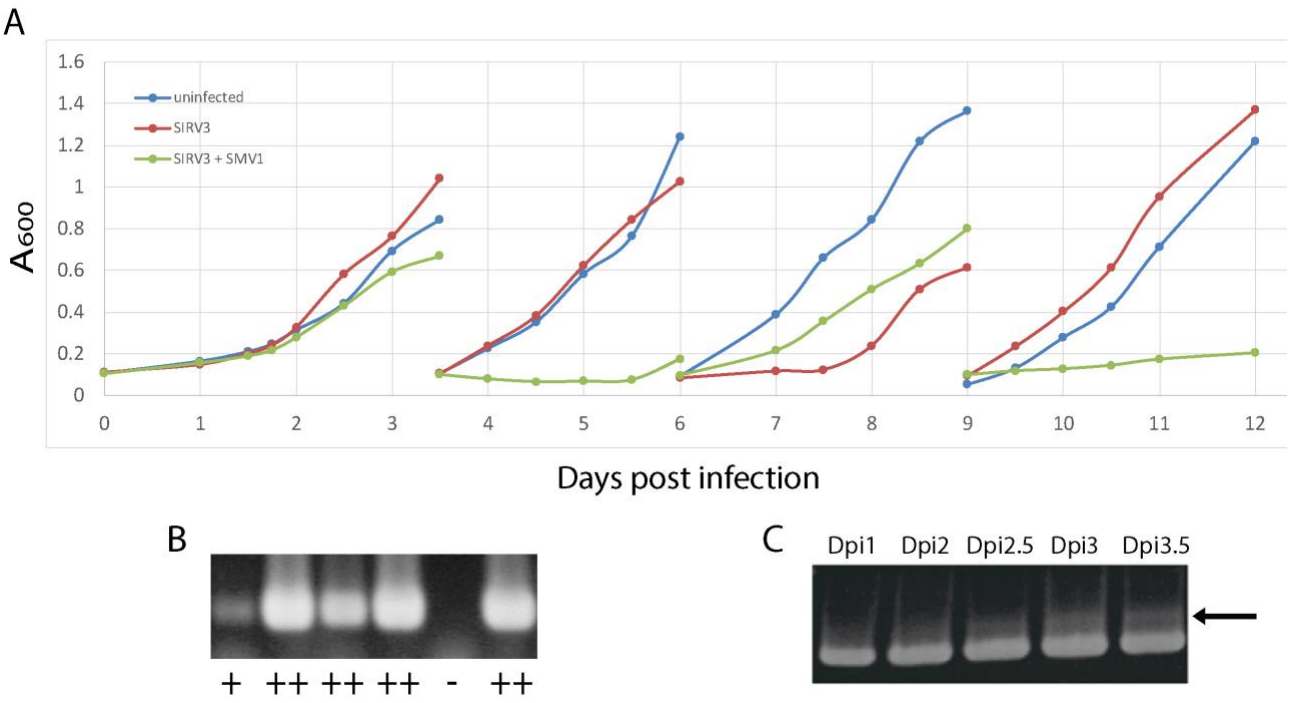

Figure S4. (A) Growth curves of the cultures uninfected, infected with SIRV3 and coinfected. 50 ml samples were diluted to A_{600} = 0.05 with fresh medium in every 3-4 days when uninfected control cultures exceeded A_{600} = 1 to prevent cell death due to nutrient deficiency. (B) A gel example illustrating how the relative viral levels presented in Table 3 were estimated visually from the gel band intensities. (C) Example depicting how spacer acquisition was initially detected by PCR amplification of the leader-end CRISPR array. Larger PCR products, indicated by the black arrow, were observed at 3 dpi and beyond.

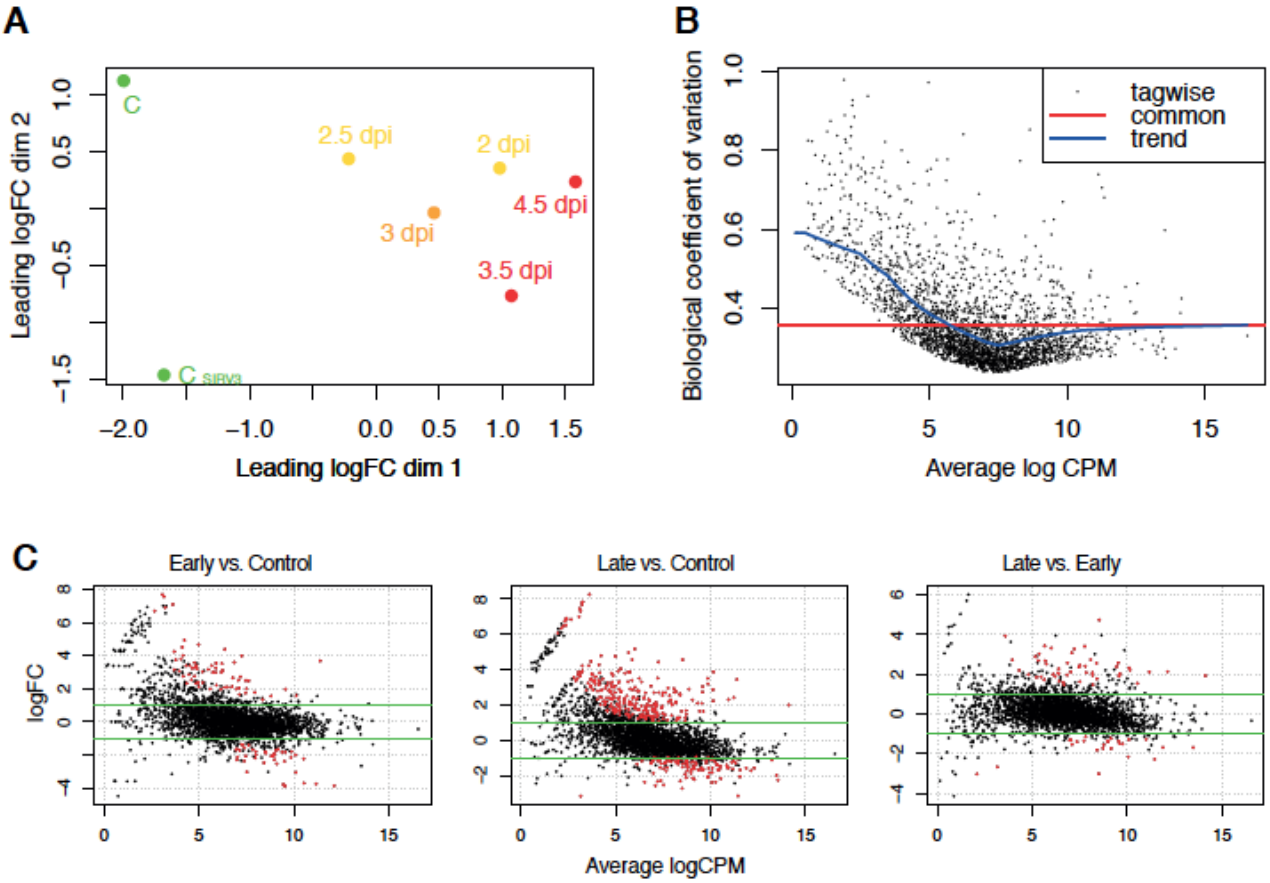

Figure S5. Differential transcription analysis and results overview. A. Multi-dimensional scaling (MDS) plot of the RNA samples. Distances correspond to leading log-fold-changes (logFC) between each pair of RNA samples. Colour codes highlight control (green), early infection (yellow), and late infection (orange and red) groups. Zero-read genes were assigned a value of 0.25 for the $\log_2$ transformation (prior.count = 0.25, *plotMDS* function from the edgeR package). C and C_{SIRV3} - controls; dpi - days post infection. B. Computed dispersion values for each gene (tagwise), transcription level (trend) and for the entire dataset (common) (*estimateDisp* function). C. Overview of differential transcription results between each group pair (*glmLRT* function); each dot represents a gene, and significantly differentially transcribed genes ($p < 0.05$) are marked in red.